

Local dynamic subgrid-scale models in channel flow 395814

By W. Cabot

1. Motivation & objectives

The dynamic subgrid-scale (SGS) model (Germano *et al.*, 1991) has given good results in the large-eddy simulation (LES) of homogeneous isotropic or shear flow, and in the LES of channel flow, using averaging in two or three homogeneous directions (the DA model). In order to simulate flows in general, complex geometries (with few or no homogeneous directions), the dynamic SGS model needs to be applied at a local level in a numerically stable way. Channel flow, which is inhomogeneous and wall-bounded flow in only one direction, provides a good initial test for local SGS models. Tests of the dynamic localization model (Ghosal *et al.*, 1993) were performed previously in channel flow (Cabot, 1993) using a pseudospectral code (Kim *et al.*, 1987), and good results were obtained. Numerical instability due to persistently negative eddy viscosity was avoided by either constraining the eddy viscosity to be positive or by limiting the time that eddy viscosities could remain negative by co-evolving the SGS kinetic energy (the DLk model). The DLk model, however, was too expensive to run in the pseudospectral code due to a large near-wall term in the auxiliary SGS kinetic energy (k) equation. One objective was then to implement the DLk model in a second-order central finite difference channel code, in which the auxiliary k equation could be integrated implicitly in time at great reduction in cost, and to assess its performance in comparison with the plane-averaged dynamic model or with no model at all, and with direct numerical simulation (DNS) and/or experimental data.

Other local dynamic SGS models have been proposed recently, e.g., constrained dynamic models with random backscatter (Carati & Ghosal, in this volume), and with eddy viscosity terms that are averaged in time over material path lines rather than in space (Meneveau *et al.*, 1994). Another objective was to incorporate and test these models in channel flow.

2. Accomplishments

2.1 Dynamic localization models in a finite-difference channel code

2.1.1 Implementation & cases

Dynamic localization (DL) models (Ghosal *et al.*, 1993) were implemented in a finite-difference code with second-order central differencing on a staggered mesh and a third-order Runge-Kutta time integration and were used to simulate channel flow for different friction Reynolds numbers, $Re_\tau = u_\tau \delta / \nu$, where ν is the molecular viscosity, δ is the channel half-width, and the friction speed u_τ is the square root of

the wall stress. Simulations were also performed using the plane-averaged dynamic (DA) model and no model at all.

In the standard dynamic model, the residual Reynolds stress that appears in the Navier-Stokes equation,

$$\tau_{ij} = \overline{u_i u_j} - \bar{u}_i \bar{u}_j \quad (1)$$

(where the overbar denotes the grid filter) is modeled with a Smagorinsky base model $(-2C\Delta^2|\bar{\mathbf{S}}|\bar{\mathbf{S}})_{ij}$, where \mathbf{S} is the strain tensor and Δ the grid filter width). The dynamic coefficient C is found by minimizing the error between the ‘‘Germano identity’’,

$$L_{ij} = \widehat{\overline{u_i u_j}} - \widehat{\bar{u}_i \bar{u}_j} \quad (2)$$

and its model terms (the caret denoting a test filter at a coarser scale than the grid filter). The error is thus

$$E_{ij} = L_{ij} + 2C\Delta^2|\widehat{\bar{\mathbf{S}}}|_{ij} - 2C\widehat{\Delta}^2|\widehat{\bar{\mathbf{S}}}|_{ij}, \quad (3)$$

where, in practice, $\widehat{\Delta} = 2\Delta$ is chosen. In the DA model, C is a global coefficient (independent of the homogeneous directions) that is found algebraically by a simple least-squares minimization of error (Lilly, 1992). In the DL model, local values of C are found by a global minimization using an iterative procedure. In the constrained dynamic localization (DL+) model, the minimization is subject to the constraint that the dynamic coefficient not be negative. Except for one simulation case, no explicit filtering was performed in the inhomogeneous wall-normal direction, and the error minimization to determine the dynamic coefficient is always performed independently in individual horizontal planes. Top-hat filters were used in all the cases discussed here.

In the unconstrained (DLk) model, an auxiliary equation for the SGS residual kinetic energy is evolved, which itself contains additional dynamic coefficients for diffusion and dissipation terms. In the finite difference code, the dissipation term in the k equation, $-C_k(\mathbf{x})k^{3/2}/\Delta$, was integrated implicitly from fractional time step j to $j+1$ by time-splitting only a linear factor of k in the expression with the remainder evaluated at the prior time step n , viz., $-1/2(k^{[j+1]} + k^{[j]})(C_k k^{1/2}/\Delta)^{[n]}$. Since $C_k \geq 0$, the latter term acts like a positive diffusion rate, making the implicit integration stable even for large time steps. As one expects physically, C_k varies roughly as y_w^{-3} near the walls; and, as found in the pseudospectral code, k varies roughly as y_w^2 even though the numerical boundary conditions only enforce a linear wall behavior (cf. Cabot, 1993).

2.1.2 Computational costs

With the DLk model, time steps approaching the convective CFL limit would now be possible with the partial implicit method were it not for large negative eddy viscosities that now arise and that must be integrated explicitly. This limits the time step, becoming a much more severe problem at higher Re_τ . For the DA and DL+ model, the (mostly) positive eddy viscosity is integrated implicitly and does

not affect the time step. The cost per time step using the DLk model (when the dynamic coefficients are computed at each time step) is about *twice* that for the DA model. At $Re_\tau = 400$, the time step also had to be 2.0 to 2.5 times smaller for the DLk model. At $Re_\tau = 1030$, the time step had to be reduced five-fold. Some expense was saved in this case by computing the dynamic coefficients every other time step. Also, fewer iterations were needed since the solution changed little from the prior time step. This resulted in the DLk simulations costing only 40% more per time step than with the DA model, hence making it seven times more expensive overall. At larger Re_τ , one can further reduce costs per step by computing dynamic coefficients at larger intervals, but the time step must still be taken increasingly smaller, which may more than offset any such savings. It appears, then, that the DLk model will generally be several times more expensive to run than simpler SGS models in this type of code.

2.1.3 LES results

Channel flow cases were examined using $Re_\tau = 180$ in a $4\pi \times 2 \times 4\pi/3$ domain (in units of δ) on $32 \times 65 \times 32$ and $64 \times 65 \times 64$ meshes (giving a spanwise resolution, in wall units, of $\Delta z^+ = Re_\tau \Delta z / \delta = 24$ and 12, respectively), and for $Re_\tau = 400$, 650, and 1030 in a $2\pi \times 2 \times 2\pi/3$ domain, on a $64 \times 65 \times 64$ mesh ($\Delta z^+ = 13$, 21, and 34, respectively).

All LES cases for $Re_\tau = 180$ on the coarse mesh ($32 \times 65 \times 32$) give mean streamwise velocities in wall units ($U^+ = U/u_\tau$) and streamwise fluctuation intensities (u_{rms}/u_τ) well in excess of the DNS results (Kim *et al.*, 1987), as seen in Fig. 1. (The DNS velocity fields were filtered by a tophat filter of the same width as the LES cases.) *Even with no model*, U^+ is slightly larger than that for DNS. Also note that no finite difference simulation at $Re_\tau = 180$ appears to give a flat log region. The DA model gives the worst overall results while the DLk model gives somewhat better results (DL+ results being intermediate). On a finer mesh ($64 \times 65 \times 64$) at $Re_\tau = 180$, it was found that SGS models have a much smaller effect (Fig. 2). Values of U^+ with no model and the DA model differ by about 6% in the log region, the latter agreeing quite well with DNS results, and the velocity intensities are also in good agreement with (filtered) DNS results. In contrast, the pseudospectral code for the same parameters and domain size on a $32 \times 65 \times 32$ mesh gives U^+ 15% below DNS results in the log region with no model and gives good agreement with the DNS results with any dynamic SGS model (Cabot, 1993). Conventional wisdom has it that spectral resolution is about twice that of finite differences on the same mesh, so the horizontal resolution for pseudospectral case should be comparable to that of the finite difference cases on the finer mesh shown in Fig. 2. (However, the wall-normal resolution for the Chebyshev expansion in the pseudospectral code and that for the second-order finite difference are probably different. Dealiasing is also usually employed in the homogeneous directions in the spectral codes.)

For $Re_\tau = 400$ (Fig. 3), the LES with no SGS model again gives U^+ about 6% below DNS (J. Kim, private communication) and the log law ($U^+ = 5.0 + 2.5 \ln y^+$); including the SGS models causes U^+ to rise close to the log law and DNS. Values of resolved velocity fluctuation intensities, with or without SGS models,

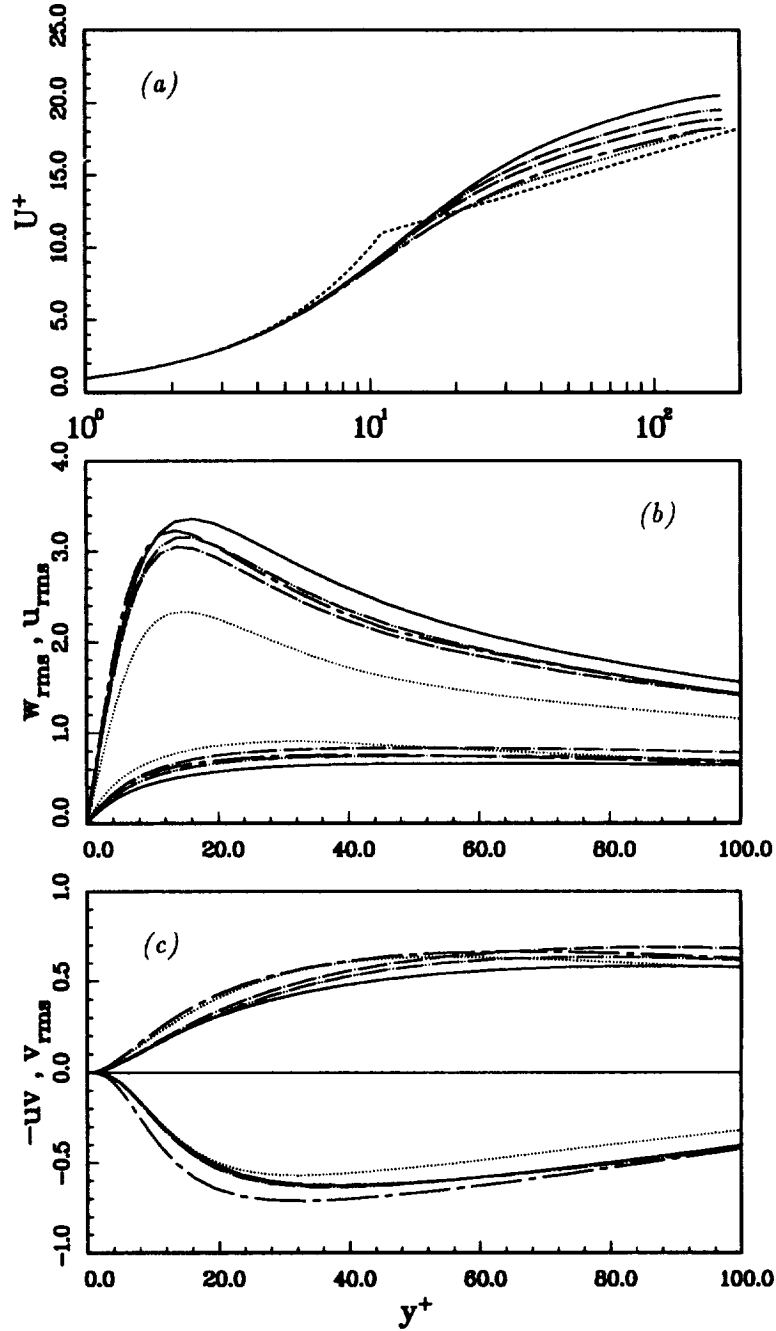


FIGURE 1. Mean streamwise velocity (a), resolved velocity intensities (b,c), and resolved Reynolds stress (c) for the LES of $Re_\tau = 180$ channel flow with the second-order finite difference code on a coarse mesh as functions of distance from the wall (all in wall units): ---- Log law, $U^+ = 5 + 2.5 \ln y^+$; DNS (filtered); and LES with ---- no SGS model, — DA model, - - - DL+ model, and - · - DLk model.

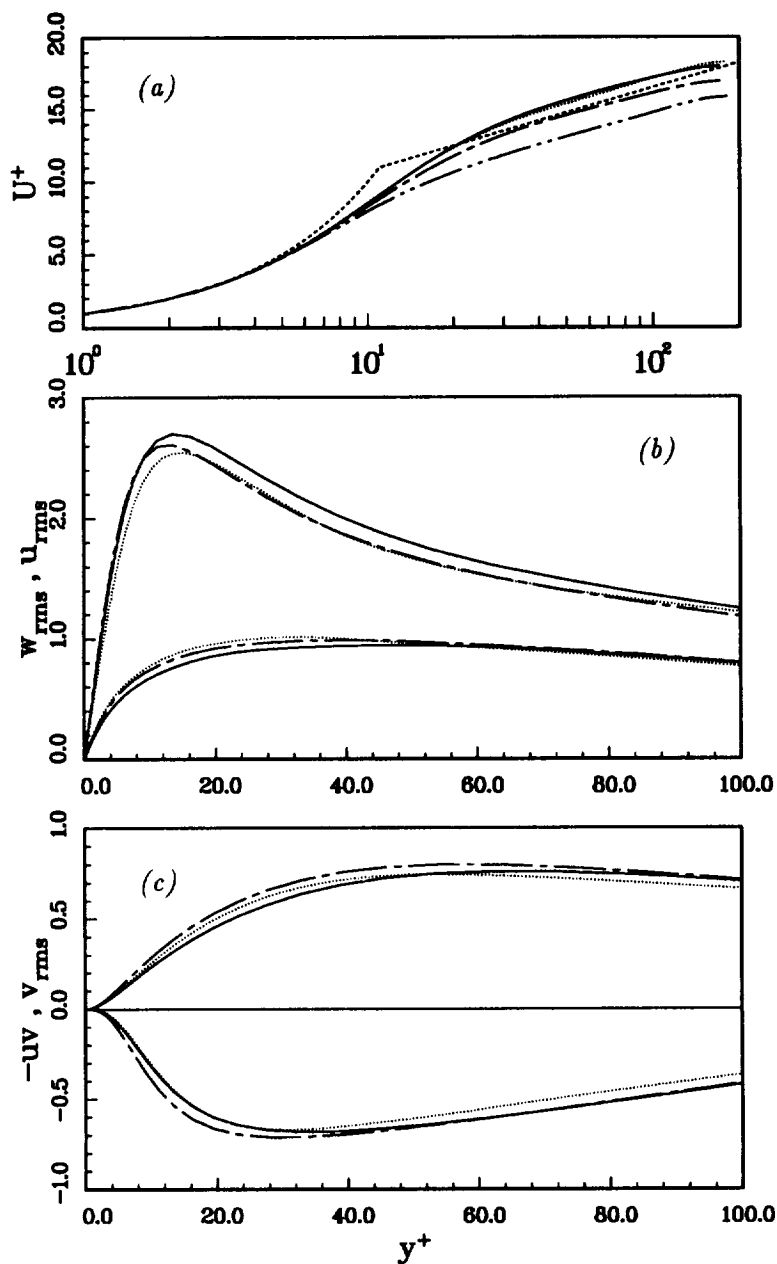


FIGURE 2. Mean streamwise velocity (a), resolved velocity intensities (b,c), and resolved Reynolds stress (c) for the LES of $Re_\tau = 180$ channel flow with the second-order finite difference code on a fine mesh as functions of distance from the wall (all in wall units): ---- Log law, $U^+ = 5 + 2.5 \ln y^+$; DNS (filtered); and LES with ---- no SGS model and — DA model. In (a), LES results from the pseudospectral code with no SGS model with comparable resolution (----) are shown; with the DA model, U^+ lies on top of the DNS results for this case.

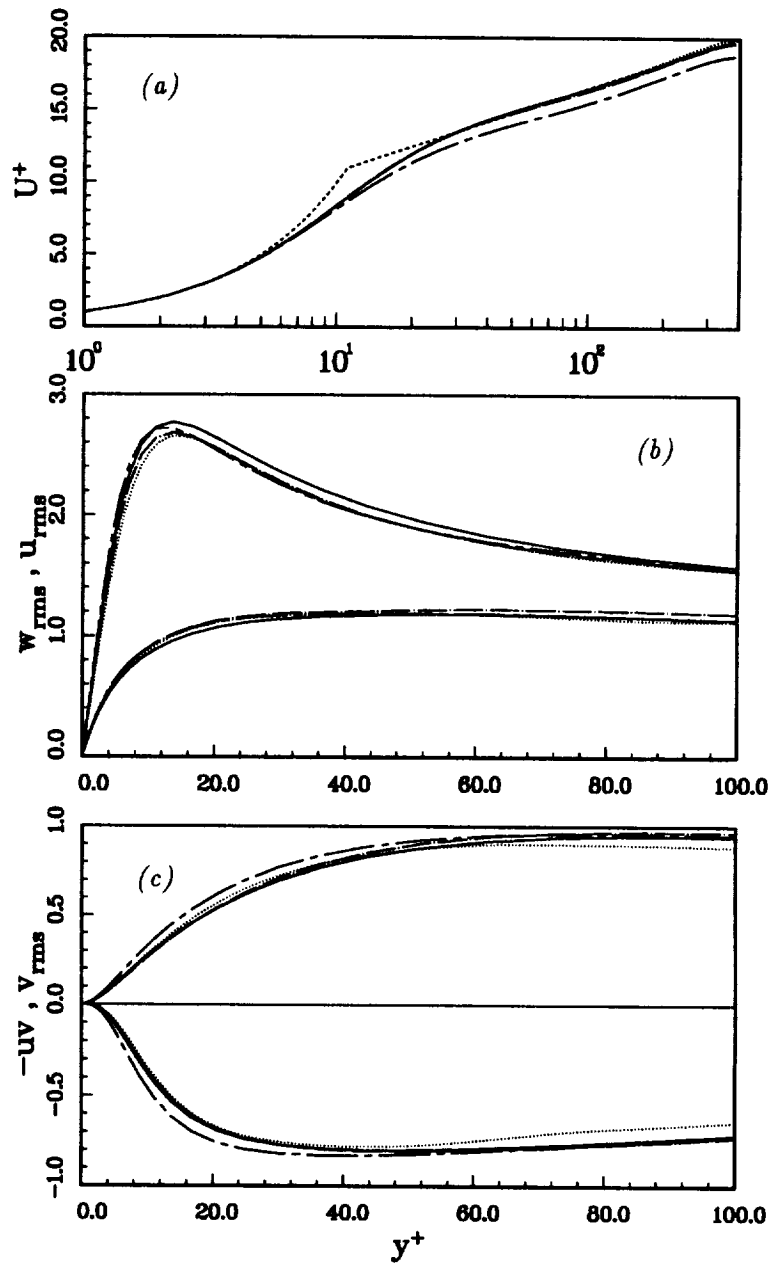


FIGURE 3. Mean streamwise velocity (a), resolved velocity intensities (b,c), and resolved Reynolds stress (c) for the LES of $Re_\tau = 400$ channel flow with the second-order finite difference code as functions of distance from the wall (all in wall units): ---- Log law, $U^+ = 5 + 2.5 \ln y^+$; DNS (filtered); and LES with ---- no SGS model, — DA model, and -·- DLk model.

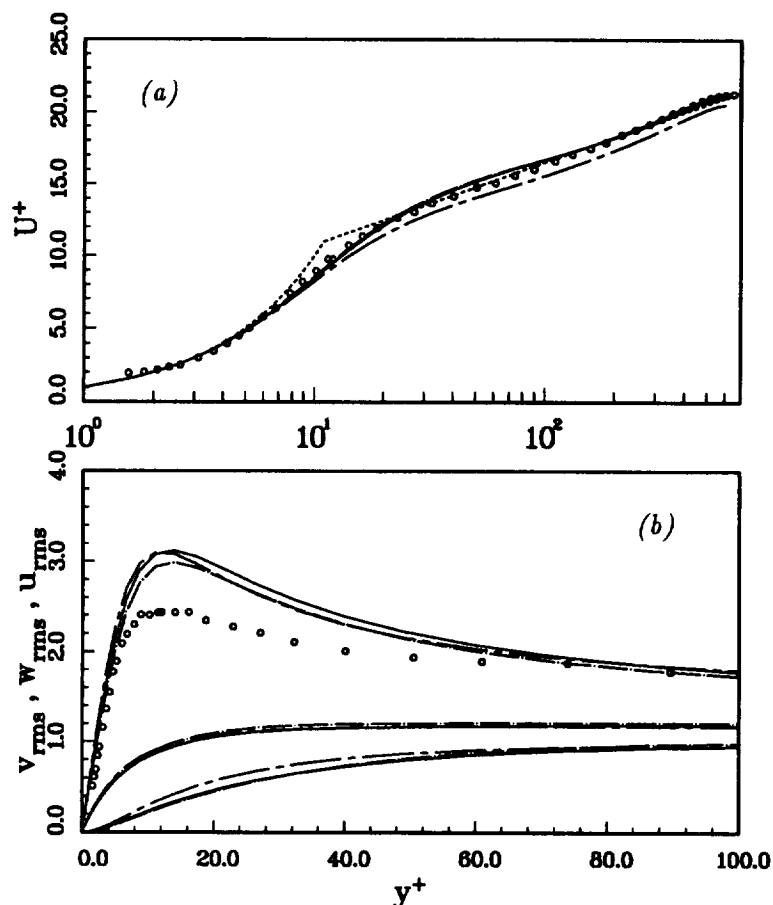


FIGURE 4. Mean streamwise velocity (a) and resolved velocity intensities (b) for the LES of $Re_\tau = 650$ channel flow with the second-order finite difference code as functions of distance from the wall (all in wall units): ---- Log law, $U^+ = 5 + 2.5 \ln y^+$; $\circ \circ \circ$ experimental data; and LES with ---- no SGS model, — DA model, and — DLk model.

agree fairly well with filtered DNS data. DA and DLk model results are almost indistinguishable. At the higher values of Re_τ , with increasingly poorer resolution, the quality of u_{rms} results degenerates considerably in comparison with experimental data by Hussain & Reynolds (1970) (Figs. 4 & 5). The presence of SGS models makes little difference to levels of velocity fluctuation intensities, with u_{rms} becoming progressively higher than experimental results in the buffer region (peaking at 3.1 and 3.6 for $Re_\tau = 650$ and 1030 simulations with the DA model and 3.0 and 3.4 with the DLk model, compared with 2.5 in the Hussain & Reynolds experiment). For $Re_\tau = 650$ (Fig. 4), U^+ is about 5% below experiment and log law with no SGS model; with SGS models it rises to the proper level in the core of the flow but develops a bump just above the buffer region. At $Re_\tau = 1030$ (Fig. 5), U^+ with no SGS model is actually on the experimental and log-law curve; additional viscosity

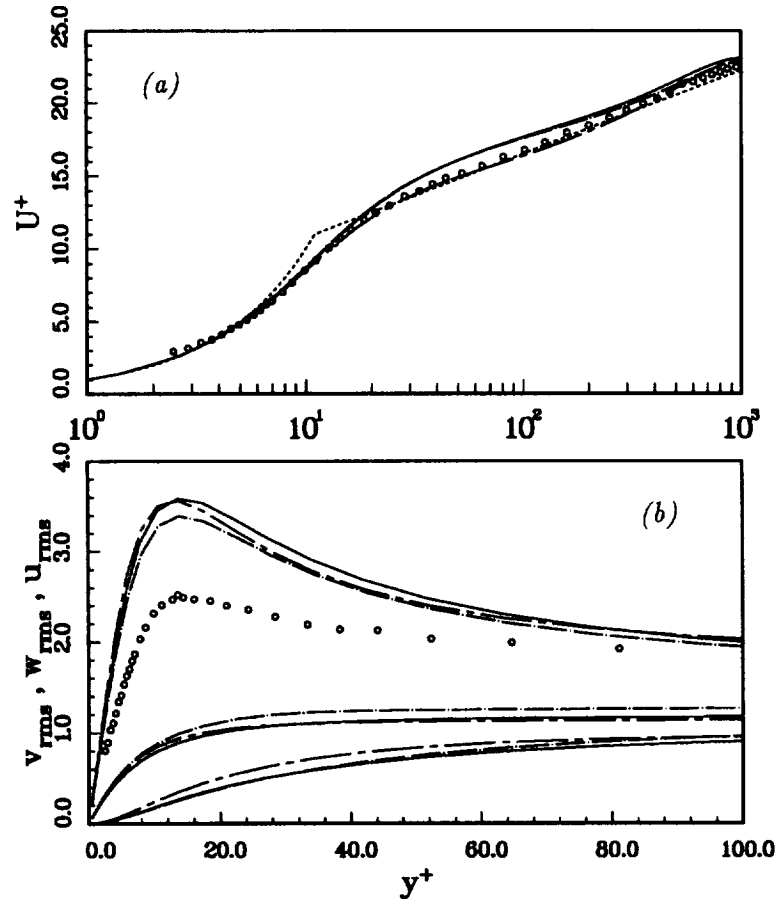


FIGURE 5. The same as Fig. 4, but for $Re_\tau = 1030$.

from the SGS models raises U^+ about 5% above this.

Note that prior LES with a DA model at $Re_\tau \approx 1400$ (using a code that was spectral in horizontal directions and used unstaggered finite differences in the wall-normal direction) gave fair agreement between U^+ and the log law (Cabot & Moin, 1993); it not only exhibited the bump beyond the buffer region, but it also gave much too large values of u_{rms} , peaking at 3.7. This LES was performed on the same domain size with a $32 \times 125 \times 64$ mesh ($\Delta z^+ = 46$). Piomelli (1993), using a pseudospectral code, found peak values of u_{rms} of 2.8 and 3.0 for $Re_\tau = 1050$ and 2000 with $\Delta z^+ = 26$ and 40, respectively, with U^+ in good agreement with the log law and experimental data.

2.1.4 Overall assessment

At coarse resolution, the second-order finite-difference scheme appears to have errors associated with it that act like extra dissipation; this causes the values of U^+ in some simulations with no SGS model to give *coincidentally* good results compared with DNS results. (The second-order statistics are less impressive.) When a SGS model is used, its (real) dissipation causes the U^+ to rise and appear to give worse

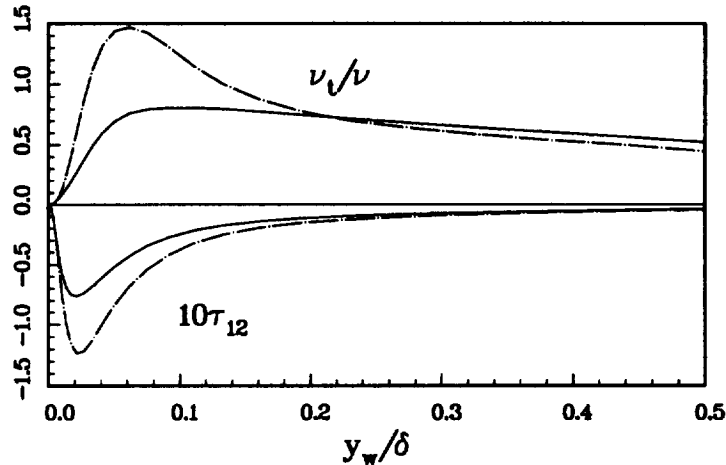


FIGURE 6. Mean eddy viscosity (scaled by the molecular value) and the mean SGS Reynolds stress (in wall units) from the wall halfway to mid-channel for $Re_\tau = 1030$ using the DA model (—) and DLk model (---).

results. There is some preliminary evidence suggesting that aliasing error in the second-order finite difference code may at least be partially responsible for these differences (A. Kravchenko, private communication). This trend persists at finer resolutions, but there the SGS model makes little difference. Indeed, the mean eddy viscosity (ν_t) predicted by dynamic SGS models in the second-order finite-difference code remains approximately equal to or less than the molecular viscosity even at the highest Reynolds numbers simulated, whereas the ν_t/ν climbs steadily with increasing Re_τ in the pseudospectral code, with peak mean values of about 5 found at $Re_\tau = 1400$. This may be caused by the removal of high-wavenumber information by the second-order finite differencing, just where the dynamic procedure samples to predict the eddy viscosity.

Mean velocity fluctuation intensities, especially the streamwise component, are more sensitive to spanwise resolution measured in wall units (Δz^+), with good results in the second-order finite-difference code for $\Delta z^+ \approx 12$, and progressively worse results for higher values. Pseudospectral codes appear to get comparable results at roughly half the horizontal resolution. Large excesses in u_{rms} (and deficits in w_{rms}) are always associated with a bump in U^+ outside of the buffer region.

In the low- Re , coarse-resolution LES, the DLk model gives somewhat better results than the DA model. But at finer resolutions and higher Reynolds numbers, there is little discernible difference in first- or second-order statistics between them, even though *mean* eddy viscosity and Reynolds stresses from the DLk model are 50–100% greater in the buffer region than those from the DA model (Fig. 6).

2.1.5 Wall-normal filtering

Tophat filtering in the wall-normal (y) direction, in addition to plane filtering, was implemented in the DA model in both finite-difference and pseudospectral codes.

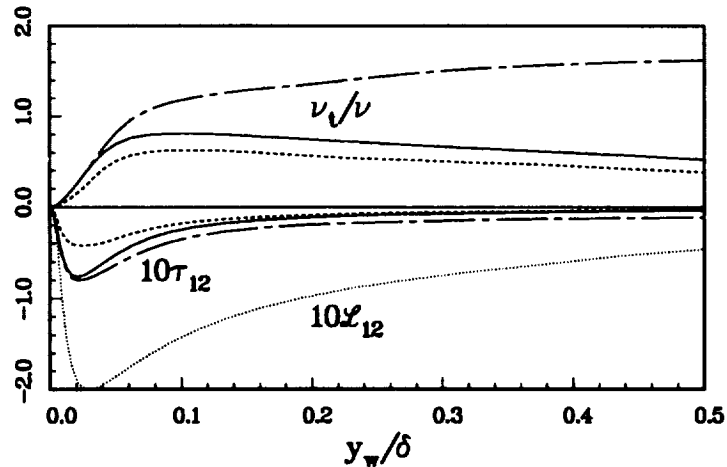


FIGURE 7. Mean eddy viscosity (scaled by the molecular value) and the mean SGS Reynolds stress (in wall units) from the wall halfway to mid-channel for $Re_\tau = 1030$ using the DA model with $\Delta = h$ and plane-filtering (—) or volume-filtering (- - -). Also shown are results from the mixed plane-filtered DA model with $\Delta = 3h/2$ (- · - ·); the Reynolds stress contribution from the (resolved-scale) Leonard term \mathcal{L}_{12} is also shown (·····) for this case.

This volume filtering causes second-order errors due to non-commutivity with spatial derivatives (cf. Ghosal & Moin, 1993). No higher-order corrections were used, which in principle are needed for the pseudospectral code but not for the second-order finite-difference code. In both codes the y -dependent dynamic coefficient $C(y)$ was removed inconsistently from the filter in the model part of Germano identity (cf. eq.[3]). In one case for the finite-difference code, C was kept consistently in the filtered expression (requiring the solution of a tridiagonal matrix for C), but this resulted in only a small ($\sim 5\%$) correction.

For the pseudospectral code at low Re_τ , the volume filtering gives eddy viscosities larger than plane filtering by only about 20% near mid-channel, the two values approaching near the walls. Results for the consistent version of the volume-filtered SGS model in the finite difference code are shown in Figs. 7 & 8 for $Re_\tau = 1030$. The eddy viscosity is seen to be increased three-fold in the interior of the channel (Fig. 7), but it approaches the plane-filtered case near the walls where the strain is greatest. For $y/\delta < 0.1$ ($y^+ < 100$), the residual stress with volume filtering is greater by less than 10% compared with plane filtering. The enhanced eddy viscosity from y -filtering has the overall effect of increasing U by a few percent (making it even worse in comparison with experimental data and the log law; see Fig. 8), with very little effect on values of velocity fluctuation intensities.

2.1.6 Explicit grid filtering

Greater numerical accuracy should be obtained in the LES when the grid filter Δ applied to the Navier-Stokes equations is much greater than the actual mesh size h (see Rogallo & Moin, 1984, and references therein). In the previous applications,

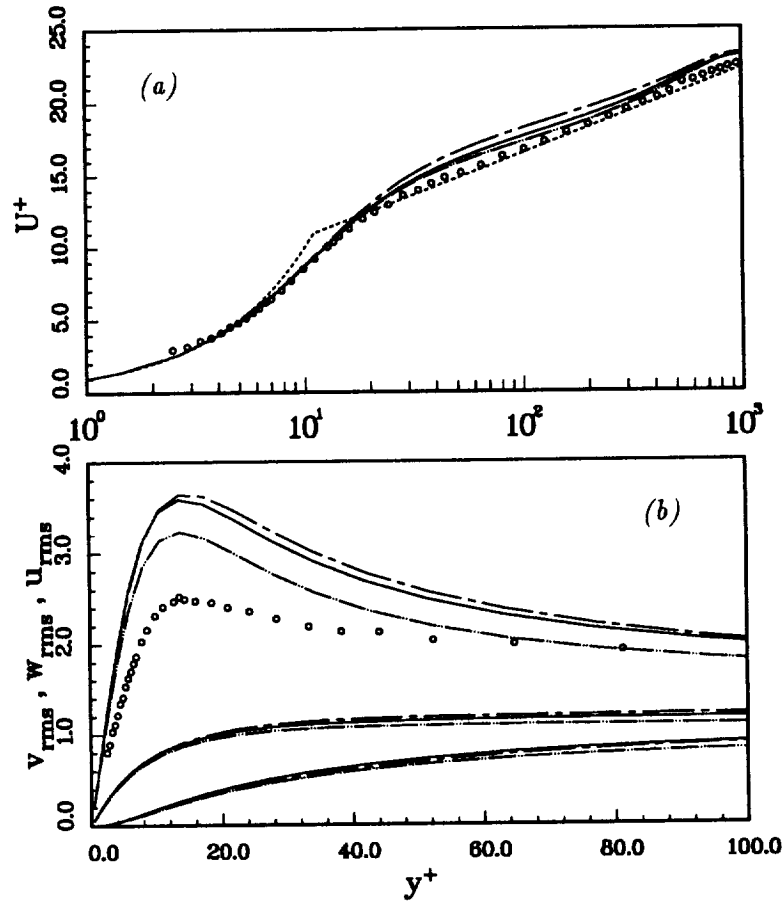


FIGURE 8. Mean streamwise velocity (a) and resolved velocity intensities (b) for the LES of $Re_\tau = 1030$ channel flow with the second-order finite difference code as functions of distance from the wall (all in wall units): ---- Log law, $U^+ = 5 + 2.5 \ln y^+$; $\circ \circ \circ$ experimental data; and LES using the DA model with $\Delta = h$ and plane-filtering (—) or volume-filtering (---), and using the mixed DA model with $\Delta = 3h/2$ and plane-filtering (— · —).

however, we have chosen $\Delta = h$ in order to minimize computation time, albeit inaccurate. A simulation with the finite difference code using the DA model was performed using $\Delta = 3h/2$ and, now, a test filter $\hat{\Delta} = 2\Delta = 3h$. (Filtering and averaging was performed only in horizontal planes with a tophat filter, and no dealiasing was used.) Information about the grid filter is communicated to the filtered linear terms in the Navier-Stokes equation only through the nonlinear Reynolds stress terms. The resolved Reynolds stress terms are influenced to some extent by the mesh on which the flow is represented, which effectively cuts off information at wavelengths shorter than the mesh size. In the standard dynamic model, the residual Reynolds stress depends only on relative differences between the test and grid filters, with no *explicit* dependence on the grid filter. Here a “mixed” dynamic SGS

model was used in which there is explicit dependence on the grid filter.

When the velocity components u_i are decomposed into filtered and residual (mostly small-scale) components, $\bar{u}_i + u'_i$, the residual stress can be written

$$\tau_{ij} = \mathcal{L}_{ij} + \mathcal{C}_{ij} + \mathcal{R}_{ij}, \quad (4)$$

where

$$\begin{aligned} \mathcal{L}_{ij} &= \overline{\bar{u}_i \bar{u}_j} - \bar{u}_i \bar{u}_j, \\ \mathcal{C}_{ij} &= \overline{\bar{u}_i u'_j + u'_i \bar{u}_j} - \bar{u}_i \bar{u}'_j - \bar{u}'_i \bar{u}_j, \\ \mathcal{R}_{ij} &= \overline{u'_i u'_j} - \bar{u}'_i \bar{u}'_j \end{aligned}$$

are the Galilean invariant Leonard, cross, and stress terms (Germano, 1986). In the mixed dynamic model, \mathcal{L}_{ij} is computed from the resolved field, and the unknown $\mathcal{C}_{ij} + \mathcal{R}_{ij}$ is fitted with a Smagorinsky model using the standard the dynamic model technique. This model has been used successfully by Zang *et al.* (1993) for flow over a cavity (although the grid filter was chosen in their case to be the same as the mesh size).

The LES of channel flow for the $Re_\tau = 1030$ case was repeated using this mixed model with $\Delta = 3h/2$. It was found that the residual stress contribution from the Leonard term is much greater than that from the dynamically modeled terms (Fig. 7). The mean streamwise velocity and the streamwise fluctuation intensity are seen in Fig. 8 to be in somewhat better agreement with experimental data using the mixed model than with the standard DA model with $\Delta = h$, but the streamwise fluctuation intensity is still too high in the buffer region.

2.2 Other local SGS models

2.2.1 Local Lagrangian model

An alternative to spatial averaging in complex flows is to use some sort of temporal averaging. Meneveau *et al.* (1994) as part of the 1994 CTR Summer Program proposed effectively to average expressions in the dynamic model in time over Lagrangian material trajectories. The local dynamic Smagorinsky coefficient C for the residual stress is estimated, neglecting (inconsistently) the filtering of C in Eq. (3), by

$$L_{ij} \sim CM_{ij}, \quad M_{ij} \equiv 2\hat{\Delta}^2 |\widehat{\mathbf{S}}| \widehat{S}_{ij} - 2\Delta^2 |\widehat{\mathbf{S}}| \widehat{S}_{ij}, \quad (5)$$

and, by least-squares fitting over components,

$$C \sim \mathbf{L} : \mathbf{M} / \mathbf{M} : \mathbf{M}. \quad (6)$$

In the ‘‘local Lagrangian’’ model, Meneveau *et al.* replaced this with

$$C \sim I_{LM} / I_{MM}, \quad (7)$$

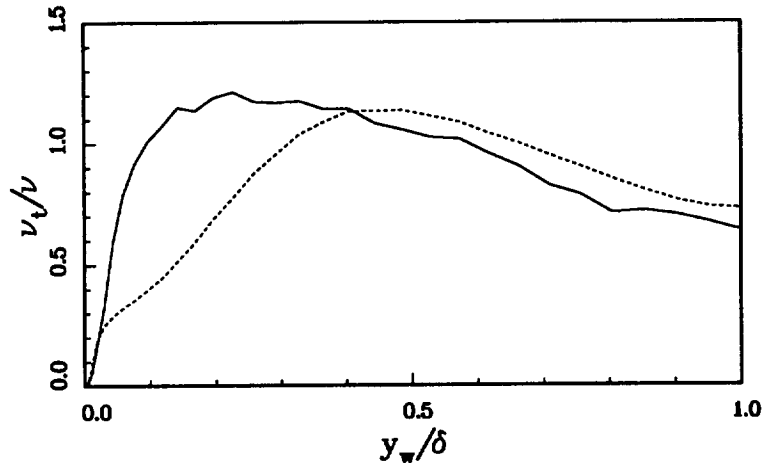


FIGURE 9. Mean eddy viscosity (scaled by the molecular value) from the wall to mid-channel for $Re_\tau = 650$ using the DA model (—) and LL model (- - -).

where I_{LM} and I_{MM} are values of $L : M$ and $M : M$ averaged over estimated Lagrangian trajectories. Note that the averaging carries full three-dimensional information, unlike the DA model in channel flow. I_{LM} was constrained to be positive to ensure numerical stability, and the time scale was chosen (somewhat arbitrarily) to be comparable to $(I_{LM})^{-1/4} \Delta$. The sensitivity of results to different Lagrangian time scales needs to be explored further.

This model was tested in homogeneous flows, and it was also implemented in a pseudospectral channel code. Simulations of fully developed turbulent channel flow with $Re_\tau = 650$ were performed with the local Lagrangian (LL) model and the standard plane-averaged (DA) model. It was found that the LL model gave significantly lower eddy viscosities above the buffer region to about $y^+ = 200$ (Fig. 9), perhaps due to ejection events from the walls, the memory of which is retained by the LL model. Wall-normal mixing in C is also evident in its near-wall behavior, varying as $y^{+2.5}$ rather than the expected y^{+3} . The lower eddy viscosities in the LL model resulted in values of U^+ lower by about 10% in the log layer than those from the DA model; the streamwise velocity intensity was also slightly lower with the LL model, peaking at 2.8 compared with 3.0 with the DA model.

A transition case was performed with an initial centerline Reynolds number of 8000 (like the LES by Germano *et al.*, 1991 and prior DNS and LES referenced therein) using both the LL and DA models. The numerical mesh was refined at several times, which also required I_{LM} and I_{MM} to be interpolated on finer grids. The test-to-filter width ratio was held constant, but $\Delta = h$ changed on remeshing, causing the values of $L : M$ and $M : M$ to shift as well. In order to reduce transients, I_{LM} and I_{MM} were also rescaled using the plane-averaged values of the revised $L : M$ and $M : M$; however, a more general technique is required for more complex flows. The LL model was generally (but not always) slightly less dissipative in the transition calculation than the DA model (Fig. 10); the exceptions appear to be a result of the LL model lagging behind the DA model in responding to higher

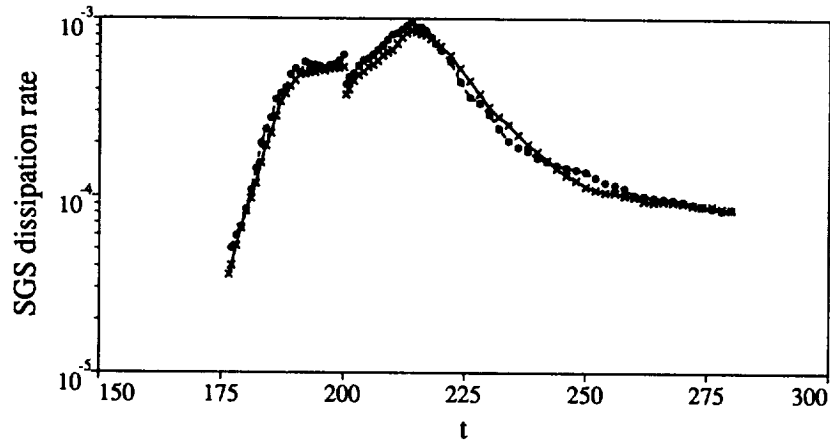


FIGURE 10. SGS dissipation rate of kinetic energy during transition in channel flow with $Re_c = 8000$: $\bullet \bullet \bullet$ DA model, $\times \times \times$ LL model. The mesh was refined at time $t = 200$ from $32 \times 65 \times 48$ to $48 \times 65 \times 64$. (All quantities are in units constructed from the initial mid-channel streamwise velocity and the channel half-width.)

turbulence levels. The LL model also gave a much more pronounced plateau in the time history of the wall stress in the peak region, which may also be due to the inherent lag of SGS stresses in the LL model. Both models gave similarly good results compared with prior LES and DNS (see Meneveau *et al.*, 1994).

2.2.2 Random backscatter model

In order to retain the realistic characteristic of backscatter of energy from the small, unresolved scales to the large, resolved scales in a local SGS model and still maintain numerical stability, Carati & Ghosal (in this volume) proposed to represent the backscatter as a random process while constraining the local eddy viscosity from the dynamic model to be non-negative (i.e., using the DL+ model). The amplitude of random forcing is related to the error in determining C locally from Eq. (3), which will be largest with the DL+ model in regions where negative values of C would arise in the unconstrained case. In Carati & Ghosal's original formulation, the amplitude of random forcing A for each component in the Navier-Stokes equation is given by

$$A^2 = [-3\hat{\mathbf{u}} \cdot (\nabla \cdot \mathbf{E})^* / \Delta t]_+, \quad (8)$$

where $(\nabla \cdot \mathbf{E})^*$ is the divergence-free derivative of the error in Eq. (3), and Δt is the time step, corresponding to an energy injection rate by the random forcing of $-\hat{\mathbf{u}} \cdot (\nabla \cdot \mathbf{E})^*$. Note that only the positive part of (8) is used so that A is defined. To make $\nabla \cdot \mathbf{E}$ divergence-free generally requires the auxiliary solution of a Helmholtz equation for a quantity related to the residual pressure; it results in a globally energy-neutral redistribution of the energy injection. The computation is cheaper (and, in most cases, not greater affected) if the divergence of $\nabla \cdot \mathbf{E}$ is retained, in

which case (8) is replaced by

$$A^2 = [-2\widehat{\mathbf{u}} \cdot (\nabla \cdot \mathbf{E}) / \Delta t]_+ . \quad (9)$$

While either formulation works well in homogeneous flow, it is found in channel flow that they generate large enough amplitudes to destabilize the numerical integration. This is because $\widehat{\mathbf{u}}$ contains a large mean flow component, and, when only positive values of A^2 are retained in (8) or (9), it gives spuriously large values (since large, offsetting negative values are discarded). One can recast $-\widehat{\mathbf{u}} \cdot (\nabla \cdot \mathbf{E})$ as $\mathbf{E} : \widehat{\mathbf{S}}$ plus diffusion terms with zero volume average. Neglecting these diffusion terms, one can recast (9) as

$$A^2 = [2\mathbf{E} : \widehat{\mathbf{S}} / \Delta t]_+ , \quad (10)$$

which gives much lower amplitudes and appears to be numerically stable in the channel flow code. Equilibrium statistics have not yet been accumulated to determine the performance of the random backscatter model.

3. Future plans

3.1 LES with random backscatter

Several channel flow simulations will be performed using the constrained dynamic localization SGS model with random backscatter (§2.3); the resulting statistics will be compared with those using other SGS models and with DNS and/or experimental data. The validity of using expression (10) instead of (8) in the framework of the formulation by Carati & Ghosal (in this volume) will be explored. The present formulation also assumes isotropy in the random forcing term, which is clearly not valid near the walls in the channel; a more general formulation will be explored to address this shortcoming, and, more pragmatically, it will be determined if in fact the channel flow is sensitive to such details in the forcing.

3.2 Second-order commutation error corrections

The correct governing equations for LES with non-uniform grids should generally include additional terms due to the non-commutation of spatial derivatives and the grid filter. Correction terms determined by Ghosal & Moin (1993) will be incorporated in a pseudospectral channel code and their effects will be determined in LES of channel flow with explicit volume filtering. The second-order commutation errors are expected to be the same order as the differencing errors in a second-order finite difference code, making it unnecessary to include them. However, the commutation terms will be included in fourth-order finite difference schemes that are being developed for LES.

3.3 Dealiased finite difference simulations

There is some evidence that aliasing errors in the second-order finite difference simulations are responsible for some discrepancies with pseudospectral results. Also, since the high-wavenumber information in second-order finite differences is known to be inaccurate, and this directly affects the results from the dynamic procedure,

simulations need to be crafted in ways that reduce this inaccuracy. Channel flow simulations will be performed with a second-order finite difference code that uses dealiasing of nonlinear products; in homogeneous directions this could be done with spectral methods, but more general procedures are required for more complex geometries. Most future simulations will be performed with grid filters that are at least twice the actual grid spacing to improve numerical accuracy of the LES, and this additional "padding" can in principle be used in the general dealiasing procedure. It will also be determined if mixed dynamic SGS models with explicit dependence on the grid filter (§2.1.6) give better results in general than the standard dynamic model for these cases.

REFERENCES

- CABOT, W. 1993 Dynamic localization and second-order subgrid-scale models in large eddy simulations of channel flow. In *Annual Research Briefs 1993*, Center for Turbulence Research, Stanford Univ./NASA Ames Research Center, 129–144.
- CABOT, W., & MOIN, P. 1993 Large-eddy simulation of scalar transport with the dynamic subgrid-scale model. In *Large Eddy Simulation of Complex Engineering and Geophysical Flows*, ed. B. Galperin & S. A. Orszag (Camb. Univ. Press).
- GERMANO, M. 1986 A proposal for a redefinition of the turbulent stresses in the filtered Navier-Stokes equations. *Phys. Fluids*. **29**, 2323–2324.
- GERMANO, M., PIOMELLI, U., MOIN, P., & CABOT, W. H. 1991 A dynamic subgrid-scale eddy viscosity model. *Phys. Fluids A*. **3**, 1760–1765.
- GHOSAL, S., LUND, T. S., MOIN, P., & AKSELVOLL, K. 1994 A dynamic localization model for large-eddy simulation of turbulent flows, *J. Fluid Mech.*, in press.
- GHOSAL, S., & MOIN, P. 1993 The basic equations for the large-eddy simulation of turbulent flows in complex geometry. *Manuscript 143*, Center for Turbulence Research, Stanford Univ./NASA Ames Research Center.
- HUSSAIN, A. K. M. F., & REYNOLDS, W. C. 1970 The mechanics of a perturbation wave in turbulent shear flow. Stanford Univ. Dept. of Mech. Eng. Rep. FM-6.
- KIM, J., MOIN, P., & MOSER, R. 1987 Turbulence statistics in fully developed channel flow at low Reynolds number. *J. Fluid Mech.* **177**, 133–166.
- LILLY, D. 1992 A proposed modification of the Germano subgrid-scale closure method. *Phys. Fluids A*. **4**, 633–635.
- MENEVEAU, C., LUND, T. S., & CABOT, W. 1994 A Lagrangian dynamic subgrid-scale model of turbulence. In *Proceedings of the Summer Program 1994*, Center for Turbulence Research, Stanford Univ./NASA Ames Research Center.

- PIOMELLI, U. 1993 High Reynolds number calculations using the dynamic subgrid-scale stress model. *Phys. Fluids A*. **5**, 1484–1490.
- ROGALLO, R. S., & MOIN, P. 1984 Numerical simulation of turbulent flows. *Ann. Rev. Fluid Mech.* **16**, 99–137.
- ZANG, Y., STREET, R. L., & KOSEFF, J. R. 1993 A dynamic mixed model and its application to turbulent recirculating flows. *Phys. Fluids A*. **5**, 3186–3196.

